A high-frequency surface-micromachined optical ultrasound transducer (SMOUT) array for 3D micro photoacoustic computed tomography (μPACT)

Zhiyu Yan*, Jun Zou
Department of Electrical and Computer Engineering, Texas A&M University, College Station, TX, 77843, USA

ABSTRACT

This letter reports a 2D high-frequency surface-micromachined optical ultrasound transducer (HF-SMOUT) array for micro-PACT (μPACT) applications. A 11 mm × 11 mm HF-SMOUT array with 220 × 220 elements (35 μm in diameter) is designed, fabricated and characterized. The center frequency and bandwidth of the HF-SMOUT elements are ~15 MHz and ~20 MHz (133%), respectively. The noise equivalent pressure (NEP) is 156 Pa (or 19 mPa/ √ Hz) within a measurement bandwidth of 5 × 75 MHz. PACT experiments are conducted to evaluate the imaging performances of the SMOUT array. Spatial resolution is estimated as 90 μm (axial) and 250—750 μm (lateral) within a 10 × 10 mm^2 FOV (field of view) and the imaging depth up to 16 mm. 3D PA image of a knotted human hair target is also successfully acquired. These results show the feasibility of using the HF-SMOUT array for μPACT applications.

Keywords: Surface micromachining; optical ultrasound transducer (OUT); high frequency ultrasound detection; photoacoustic (PA); computed tomography (CT)

1. INTRODUCTION

As a hybrid modality, photoacoustic (PA) imaging has been utilized to acquire both structural and functional information of biological tissues [1]. To resolve fine details at penetration depths beyond optical diffraction limit, detection of high-frequency PA signals is required. With a single-element focused transducer, photoacoustic microscopy (PAM) can achieve high resolution but only within the focal zone of the transducer [2]. Alternatively, with a high-frequency 2D transducer array, micro photoacoustic computed tomography (μPACT) can resolve small features at mm depth without significant out-of-focus degradation [3]. Currently, piezoelectric transducer arrays are mostly used for PACT due to its wide availability [4]. However, as the operation frequency and number of the transducer elements increase, the (electrical) ultrasound receiver could become extremely complex and costly. To address this issue, optical ultrasound transducer (OUT) arrays have been developed [5]. They have good responsivity even at high ultrasound frequencies [6] and can be read out wirelessly with free space optics. However, non-uniform element performance remains a fundamental issue in current OUT arrays [7]. As a result, element-wise tuning of the interrogation optical wavelength is needed when reading out the ultrasound signals from multiple elements, which seriously limits the data acquisition speed.

Recently, we have demonstrated a new 2D surface-micromachined optical ultrasound transducer (SMOUT) array with high uniformity and stability, thereby making the tuning of the interrogation wavelength unnecessary [8]. As shown in Fig. 1(a), a SMOUT element is a vacuum-sealed Fabry-Perot (FP) cavity consisting of two identical DBRs (distributed Bragg reflectors). The top DBR consists of a suspended diaphragm that can be vibrated in the presence of impinging ultrasound waves. Such vibrations change the cavity length of the SMOUT element and shift its reflectivity spectrum, which can be read out as fluctuation in the reflected optical intensity (Fig. 1(b)). However, the center frequency of the SMOUT array is only ~3.5 MHz, which is too low for conducting μPACT. In this letter, we report on the development of a new high-frequency SMOUT (HF-SMOUT) array. Ultrasound and photoacoustic experiments are conducted to characterize the acoustic performances of the HF-SMOUT array, including center frequency, bandwidth and sensitivity. The HF-SMOUT array is also used to acquire PA images of various targets to demonstrate its imaging capabilities. The results have shown that the HF-SMOUT array has high sensitivity and wide bandwidth, making it a promising solution for μPACT applications.

Photons Plus Ultrasound: Imaging and Sensing 2024, edited by Alexander A. Oraevsky, Lihong V. Wang, Proc. of SPIE Vol. 12842, 1284204 · © 2024 SPIE
1605-7422 · doi: 10.1117/12.3000769

2. SENSOR DESIGN AND FABRICATION

Functioning based on the optomechanical modulation (Figs. 1 (a) &(b)), the center frequency (i.e., resonance frequency of the diaphragm) of a SMOUT element is determined by the material properties and dimensions of the diaphragm. A diaphragm with smaller diameter and larger thickness resonates at higher frequency. Because it also affects the read-out wavelength of the SMOUT element, the thickness of the DBR diaphragm is kept as a constant (e.g., ~1.4 μm) [8]. FEM (finite-element method) simulation is conducted with COMSOL Multiphysics to estimate the resonance frequency of the DBR diaphragm with different diameters from 20 μm to 50 μm (with 5-μm increment) and the results are plotted as Fig. 1 (c). A diaphragm with smaller diameter resonates at higher frequency, yet the ultrasound sensitivity is decreased due to the smaller displacement. To achieve detection frequency higher than 20 MHz and maintain good sensitivity, the diameter of the SMOUT element is set to be 35 μm (as shown in Fig. 1 (c)). Four 11 mm × 11 mm HF-SMOUT arrays are fabricated with a surface micromachining process [8]. To maximize the filling factor of the arrays, the pitch size is set as 50 μm (Fig. 1 (d)). The sub-figure in Fig. 1 (d) shows a 2 × 2 element array. The total number of elements in each HF-SMOUT array is 220 × 220. A silicon dioxide/nitride DBR is first deposited on a glass substrate by chemical vapor deposition. A zinc oxide film (as sacrificial layer) is then deposited and patterned, followed by the deposition of another DBR which is identical to the first one. After removing the sacrificial layer, the top DBR is released as a suspended diaphragm. A layer of Silicon dioxide is coated with chemical vapor deposition to hermetically seal the SMOUT element. Lastly, each SMOUT element is coated with a 3-μm-thick Parylene-C film for encapsulation.

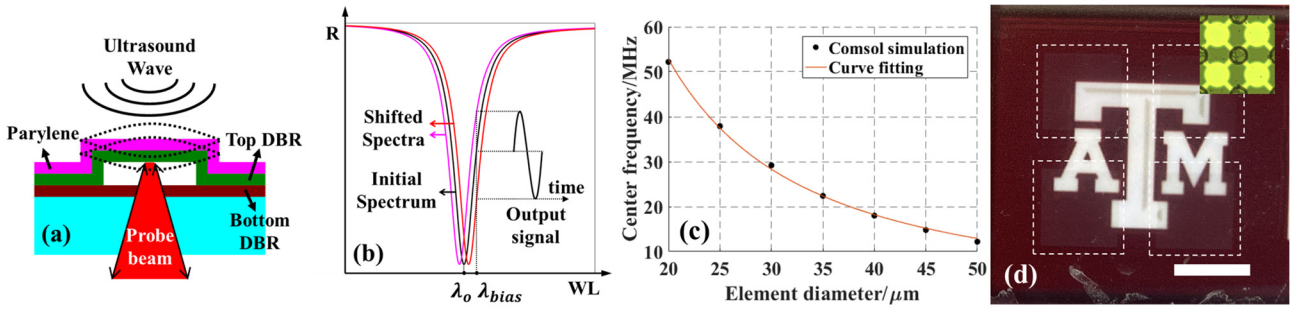

Fig. 1. (a) Schematic showing the cross-section and ultrasound detection mechanism of a SMOUT element. (b) Schematic showing the modulation of reflectivity at interrogation wavelength $\lambda_{\_bias}$ by acoustic-induced reflection spectrum shift. (c) COMSOL simulation results showing the relationship between center frequency and element diameter. (d) Top view showing four identical HF-SMOUT arrays marked out with white dashed boxes (the scale bar is 1 cm; the subfigure shows 2 × 2 HF-SMOUT elements).

3. TESTING AND CHARACTERIZATION

3.1 Experimental setup

An optical setup is built to characterize the ultrasound detection performances of the HF-SMOUT elements (Fig. 2) [8]. The interrogation light source is a fiber-coupled wavelength-tunable CW laser (BS-785-1-HP, Superlum). The laser output is coupled into a single-mode fiber circulator (Precision Micro-Optics) and collimated by a fiber collimator (F810APC-780, Thorlabs). The collimated laser beam is focused by a 10× objective lens before illuminating the HF-SMOUT elements. The reflected light from the illuminated HF-SMOUT element is coupled back into the circulator and guided to a photo receiver (DET36A, Thorlabs). After being read out by the photo receiver, the voltage signal is amplified by a pulser/receiver (5073PR, Olympus) and acquired by a DAQ board (ATS9350, AlazarTech). To monitor the focusing and alignment of the interrogation laser spot, light from a Halogen light source (HL-2000-LL, Ocean Insight) is combined with the interrogation laser by a dichroic mirror (DMLP650, Thorlabs). 1% of the reflected light power from the SMOUT array is projected to a CCD camera by a beam sampler (BSF10-A, Thorlabs) to image the laser spot and the interrogated element. The SMOUT array is placed above an acoustic source with the device side immersed in water (for acoustic matching). By using two linear motorized stages (NRT100, Thorlabs), the interrogation laser spot is scanned over the array for data collection. A desktop computer is used for data storage, processing, and automatic control of the setup.

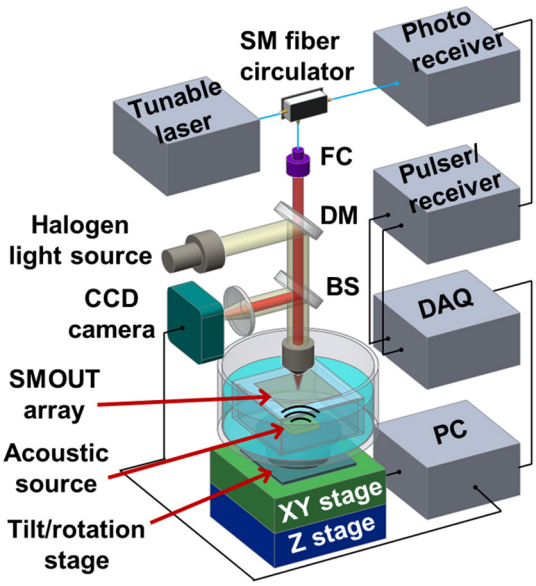

Fig. 2. Experimental setup for HF-SMOUT interrogation

3.2 Acoustic characterization

Photoacoustic (PA) testing is conducted to characterize the frequency response of the HF-SMOUT array. Black human hairs are chosen as PA targets for their high optical absorption [9]. A human hair is illuminated by a 532-nm pulsed laser with ~3 ns pulse width and ~150 μJ pulse energy (FQS-200-1-532, Elforlight Ltd) to excite PA waves. The human hair is located 10 mm beneath the SMOUT device. Fig. 5a shows the typical PA response of an HF-SMOUT element (Fig. 3 (a)). Its frequency spectrum after FFT (fast Fourier transform) is shown in Fig. 3 (b). The center frequency of the SMOUT element is ~14 MHz with a bandwidth ~18 MHz (129%). The peak at 11 MHz is due to the artifact caused by the resonance of the human hair target. Additionally, the "long tail" of the PA signal (in Fig. 3 (a)) is partially due to the crosstalk of the adjacent elements [10]. The NEP (noise equivalent pressure) of the element is also measured by using a 15-MHz flat piezoelectric transducer as the ultrasound source (Olympus). The flat transducer is located 15 mm beneath the HF-SMOUT array. A representative signal read out from one HF-SMOUT element is shown in Fig. 3 (c). Repeating the testing on 5 adjacent elements (receiving similar ultrasound pressure) shows a rms (root mean square) signal amplitude of 2.16 V. The noise of the system is measured as 0.86 mV (with 16 signal averaging) within a measurement bandwidth of 5—75 MHz. The corresponding acoustic pressure is measured as 390.7 kPa with a 0.2-mm needle hydrophone (NH0200, Precision Acoustics). Based on these results, the NEP of the HF-SMOUT element is estimated as 156 Pa (or 19 mPa/ √ Hz) within the measurement bandwidth (with 5 mW incident power).

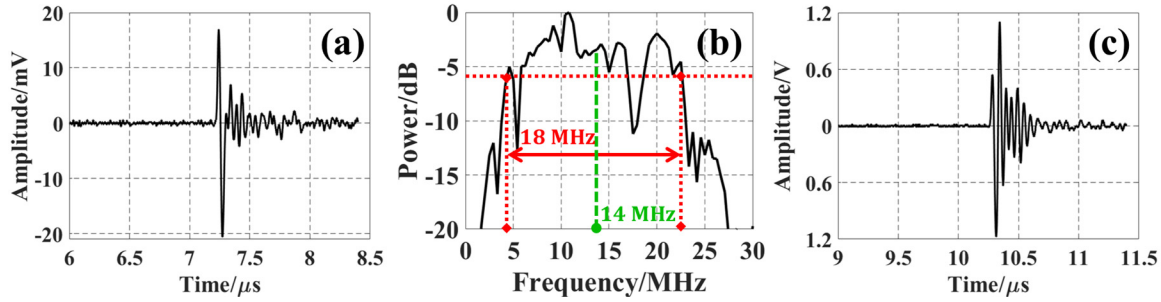

Fig. 3. (a) Representative PA signal received from the black hair target, (b) the FFT spectrum of the PA signal as the estimation of HF-SMOUT's frequency response, and (c) a representative ultrasound signal with a flat transducer as source for NEP measurement.

3.3 Temperature and temporal stability

To characterize the thermal and temporal stability of the HF-SMOUT array, the shift of ORW is monitored when the front surface of the HF-SMOUT array is immersed in water and under different temperature. Firstly, ambient temperature is

controlled by heating up the entire water tank with a hot plate. ORWs of five adjacent elements are recorded under different temperatures (Fig. 4 (a)). The ORW rms values show a standard deviation of 0.45 nm within a temperature range of 25—55 °C. Secondly, the ORWs of the five elements are measured continuously for 7 days with a standard deviation of 0.93 nm (Fig. 4 (b)).

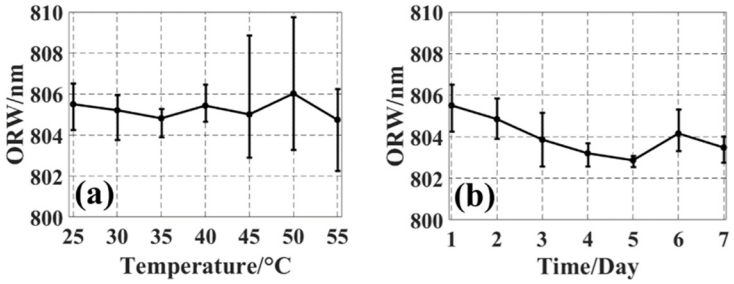

Fig. 4. RMS value of ORWs of three tested HF-SMOUT elements (a) at different ambient temperature and (b) immersed in water for seven consecutive days. Error bars are included in both plots to show the deviation of the ORW.

4. IMAGING EXPERIMENT

To demonstrate the PACT capability of the HF-SMOUT array, an imaging setup is built, as illustrated in Fig. 5 (a). PA data acquisition is conducted by scanning the interrogation laser spot over the entire array area, throughout which the laser spot is aimed at the center of each single element. With the acquired PA data, PA images of the targets are reconstructed by utilizing the k-space method [11]. Three black human hairs (Target 1, 2 and 3 in Fig. 5 (b)) are imaged to characterize the HF-SMOUT's spatial resolution. The hairs are parallelly aligned along the Y axis. They are located at the depth of 6 mm, 11 mm and 16 mm, respectively, and are separated approximately 1.5 mm away from each other along the X axis. 1D scanning of the probe laser spot over a linear array of HF-SMOUT elements along the X axis is conducted with maximal spatial sampling frequency (i.e., every single element) to obtain a 2D tomography of the three targets within the X-Z plane. Fig. 5 (c) shows the reconstructed 2D B-mode PA image of the three hair targets highlighted by the red dashed circles. The intensity profiles of the PA image along Z axis, which is also the PSF (point spread function) along Z axis, is plotted in Fig. 5 (d). By analyzing the FWHM (full width half maximum) of the PSF, the axial resolution is estimated to be ~90 μm at all the three depths, which is mainly determined by the center frequency and bandwidth of the HF-SMOUT element. Similar analysis is also done along X axis to evaluate the lateral resolution (Fig. 5 (e)). The lateral resolution is estimated as 250 μm, 450 μm and 750 μm at the depth of 6 mm, 11 mm and 16 mm, respectively. The lateral resolution is not as good as the axial resolution, partially because it is also affected by the limited view angle [12] due to the finite size and planar geometry of the HF-SMOUT array. Degradation of the lateral resolution is also expected at larger depth due to smaller view angle.

To further evaluate the HF-SMOUT array's ability for high-resolution 3D imaging of targets with arbitrary geometry, a second imaging experiment with a knotted human hair as target is conducted. As shown in Fig. 6 (a), the knotted hair, with the lateral size of ~ 3 mm, is placed ~5 mm beneath the HF-SMOUT array. The diameter of the pulsed excitation laser is adjusted to ~3 mm to illuminate the entire hair knot. PA data are acquired through a 2D scanning over the entire HF-SMOUT array (11 mm × 11 mm) with a step of 0.2 mm. The reconstructed 3D image of the knotted hair is shown in Fig. 6 (b), which matches well with the target. A small part of the target (on the left end) is missing from the image, possibly because it is not properly illuminated by the excitation laser beam.

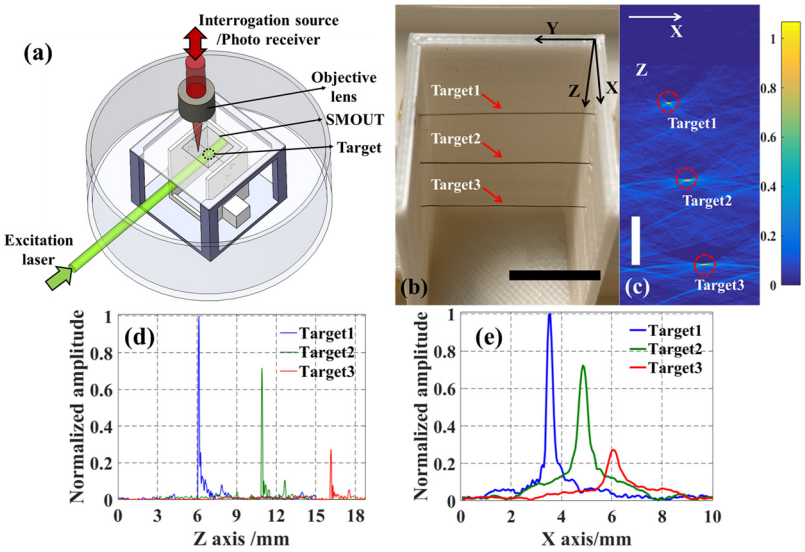

Fig. 5. (a) Experimental setup for μ-PACT imaging. (b) Three pencil lead targets (scalebar 10mm). (c) 2D reconstructed PA image of the three black hair targets (scalebar 5 mm). Amplitude profile of the 2D image along Z axis (d) and X axis (e) for analysis of axial and lateral resolution, respectively.

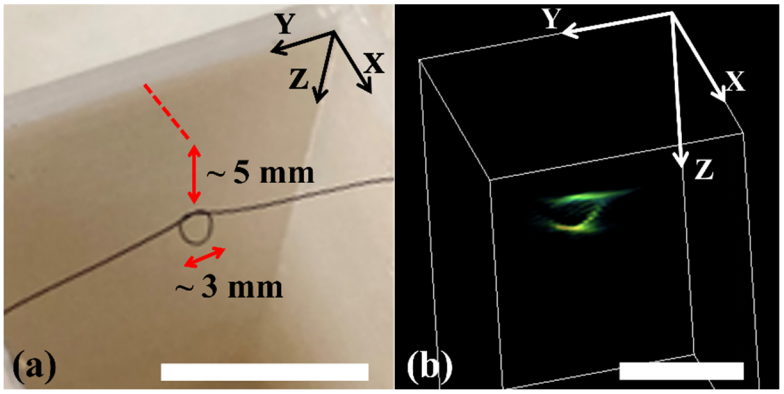

Fig. 6. (a) A knotted hair as target for PACT experiment; and (b) the reconstructed 3D PA image (scale bars in both figures represent 5 mm)

5. CONCLUSION

In conclusion, a new HF-SMOUT array has been designed, fabricated, and characterized. The testing results have shown that the HF-SMOUT array has wide acoustic bandwidth and high acoustic sensitivity. PACT experiments have been conducted to evaluate the imaging performances of the HF-SMOUT array, which show good FOV, large imaging depth and high axial resolution. As a result, the HF-SMOUT array could provide a promising solution for 3D μPACT applications. To increase the detection frequency of the HF-SMOUT array, the size of each element needs to be further reduced, which however will lower its detection sensitivity. This can be compensated for by increasing the optical power of the interrogation light. In addition, trenches or buffering structures can be fabricated around each SMOUT element to reduce the crosstalk of adjacent elements and improve their acoustic bandwidth. The lateral resolution can be further improved by scanning a larger SMOUT array or a curved array (fabricated on flexible substrates). New data acquisition approaches will need to be developed to handle the larger number of elements and also non-planar array configuration.

ACKNOWLEDGMENTS

This work was supported in part by the National Science Foundation (ECCS-1809710, ECCS-2330199, CMMI-1852184, and CBET-2036134).

REFERENCES

[1] L. V. Wang, Photoacoustic Imaging and Spectroscopy, vol. 24, Boca Raton, FL: CRC Press, 2009, p. 121909.
[2] Cheng Fang and Jun Zou, "Acoustic-resolution photoacoustic microscopy based on an optically transparent focused transducer with a high numerical aperture," Opt. Lett. 46, 3280-3283 (2021).
[3] L. Deng, X. He, J. Zhang, G. Liu, S. Han, Y. Lou, L. Zeng and X. Ji, "Ultra-compact micro-photoacoustic tomography for brain imaging in vivo," Appl. Phys. Lett. 119 (21), 213701 (2021).
[4] J. Xia and L. V. Wang, "Small-Animal Whole-Body Photoacoustic Tomography: A Review," IEEE. Trans. Biomed. Eng. 61 (5), 1380-1389 (2014).
[5] G. Wissmeyer, M. A. Pleitez, A. Rosenthal and V. Ntziachristos, "Looking at sound: optoacoustics with all-optical ultrasound detection," Light Sci Appl 7, 53 (2018).
[6] E. Zhang, J. Laufer and P. Beard, "Backward-mode multiwavelength photoacoustic scanner using a planar Fabry-Perot polymer film ultrasound sensor for high-resolution three-dimensional imaging of biological tissues," Appl. Opt. 47 (4), 562-577 (2008).
[7] P. C. Beard, "Two-dimensional ultrasound receive array using an angle-tuned Fabry-Perot polymer film sensor for transducer field characterization and transmission ultrasound imaging," IEEE T. Ultrason. Ferr. 52(6), 1002-1012 (2005).
[8] Z. Yan and J. Zou, "Large-scale surface-micromachined optical ultrasound transducer (SMOUT) array for photoacoustic computed tomography," Opt. Express 30(11), 19069-19080 (2022).
[9] R. Ansari, E. Zhang, A. Desjardins and P. Beard, "All-optical forward-viewing photoacoustic probe for high-resolution 3D endoscopy," Light Sci Appl 7, 75 (2018).
[10] G. Gurun, P. Hasler and F. L. Degertekin, "Front-end receiver electronics for high-frequency monolithic CMUT-on-CMOS imaging arrays," IEEE T. Ultrason. Ferr. 58(8), 1658-1668 (1993).
[11] B. E. Treeby and B. T. Cox, "k-Wave: MATLAB toolbox for the simulation and reconstruction of photoacoustic wave-fields," J. Biomed. Opt. 15(2), 021314 (2010).
[12] Chao Tian, Chenxi Zhang, Haoran Zhang, Dan Xie and Yi Jin, "Spatial resolution in photoacoustic computed tomography," Rep. Prog. Phys. 84, 036701 (2021).